

# Enhanced Isopropyl Alcohol Conversion over Acidic Nickel Phosphate-Supported Zeolite Catalysts

Hasanudin Hasanudin,\* Wan Ryan Asri, Lola Andini, Fahma Riyanti, Ady Mara, Fitri Hadiah, and Zainal Fanani



Cite This: *ACS Omega* 2022, 7, 38923–38932



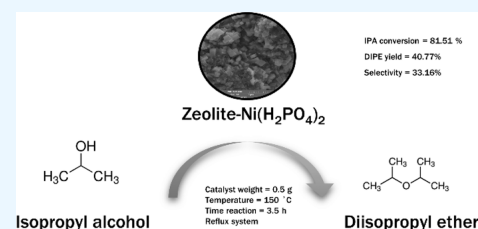
Read Online

ACCESS |

Metrics & More

Article Recommendations

**ABSTRACT:** In this preliminary research, the catalytic activity of isopropyl alcohol conversion to diisopropyl ether through dehydration reaction catalyzed by zeolite-Ni and zeolite-Ni(H<sub>2</sub>PO<sub>4</sub>)<sub>2</sub> was comparatively described. The natural zeolite was treated with 1% HF and 6 N HCl prior to modifications using the impregnation method. Isopropyl alcohol conversion was examined at a mild temperature of 150 °C for 3.5 h on the reflux system with various catalyst loadings. X-ray diffraction and Fourier transform infrared analysis confirmed the successful impregnation of nickel and nickel phosphate into the zeolite. Scanning electron microscopy analysis revealed a cubic-like structure on zeolite-Ni(H<sub>2</sub>PO<sub>4</sub>)<sub>2</sub>, whereas homogeneously distributed nickel species were observed on the zeolite-Ni catalyst. Energy-dispersive X-ray spectroscopy analysis reinforced the accomplishment of zeolite modifications. The N<sub>2</sub> physisorption isotherms showed a decline in the surface area and total pore volume of the zeolite because of the blocking of pores. The zeolite-Ni(H<sub>2</sub>PO<sub>4</sub>)<sub>2</sub> catalyst had higher acidity than unmodified zeolite and zeolite-Ni catalysts, which inherently suggested that the presence of phosphate groups results in higher catalytic activity toward isopropyl alcohol. The highest catalytic activity was attained by 8 mEq/g metal loading zeolite-Ni(H<sub>2</sub>PO<sub>4</sub>)<sub>2</sub> with isopropyl alcohol conversion of 81.51%, diisopropyl ether yield, and selectivity of 40.77 and 33.16%. The reusability study suggested that the zeolite-Ni(H<sub>2</sub>PO<sub>4</sub>)<sub>2</sub> catalyst was still active and had sufficient catalytic activity stability toward isopropyl alcohol after the third cycle was reused. This nickel phosphate-based modified zeolite was adequately potential for diisopropyl ether production through isopropyl alcohol dehydration.



## INTRODUCTION

Nowadays, there has been a pronounced motivation to improve the combustion efficiency of gasoline pools as this condition is related to the accumulation of pollutants emitted during the combustion process.<sup>1</sup> Recently, oxygenate compounds such as ethyl *tert*-butyl ether (ETBE), methyl tertiary butyl ether (MTBE), tertiary amyl methyl ether (TAME), and diisopropyl ether (DIPE) have been employed as gasoline additives because they can enhance the cleaner combustion process.<sup>2</sup> This ether-based fuel additive diminishes hazardous emissions such as NO<sub>x</sub>, CO<sub>x</sub>, and HC<sub>x</sub> and also increases the octane number of fuel that offers a sustainable fuel additive than other ethanol-based ones.<sup>3</sup> However, the toxic and high soluble water properties of MTBE are crucial drawbacks, preventing this fuel additive from being continuously used because it contaminates soil groundwater,<sup>4</sup> whereas ETBE and TAME are likely economically feasible,<sup>5</sup> but their inadequate stock can cause considerable problems. Among the available options, DIPE appears to be a viable alternative as a gasoline additive because it leads to cleaner production with a nonpolluting chemical.<sup>3,6</sup> In addition to improving the octane number of gasoline, DIPE has better compatibility with high oxygen content, resulting in better combustion conditions.<sup>7,8</sup>

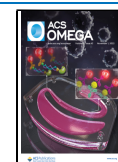
Moreover, adequate blending properties and its lower solubility in water make DIPE a reasonably efficient substitute compared with other gasoline additives.<sup>9</sup> Some studies have reported that DIPE could minimize the knocking in the combustion of HCCI,<sup>10</sup> while the test of engines containing DIPE and gasoline blend has confirmed the viability of DIPE.<sup>11</sup>

Currently, DIPE can be produced through the dehydration of alcohol using a heterogeneous catalyst. In this context, a wide type of catalysts such as iron and alumina,<sup>7</sup> Ni–Cu–Cr and Ni–Cu-loaded H-β-zeolite,<sup>9</sup> carbon acid,<sup>12</sup> Pt-promoted CuO/TiO<sub>2</sub>-ZrO<sub>2</sub>,<sup>13</sup> Ru- and Pd-supported N-doped carbon nanotubes,<sup>14</sup> crystalline heteropolyacids,<sup>15</sup> Al<sub>2</sub>O<sub>3</sub>-TiO<sub>2</sub>,<sup>16</sup> SiO<sub>2</sub>-ZrO<sub>2</sub>,<sup>17</sup> Ni-W sulfides,<sup>18</sup> and (WO<sub>3</sub>)<sub>n</sub> and (MoO<sub>3</sub>)<sub>n</sub><sup>19</sup> have been extensively employed, which show various catalytic activities. Presently, natural alumina silicate-based catalysts such as zeolites and clays are promisingly auspicious because

Received: July 22, 2022

Accepted: October 10, 2022

Published: October 18, 2022



they are economically favorable, abundantly available, and have adequate catalytic active sites, which have catalyzed various reactions. Zeolites are readily preferred over other acid catalysts because of their wide pore size distribution, thermal stability, and selectivity on the desired product.<sup>9</sup> Various zeolite-based catalysts, including ZSM-5, SAPO-34, mordenite, AlPO-4, and clinoptilolite, have been revealed to be active in the alcohol-involved dehydration reaction.<sup>20</sup> However, the product selectivity to DIPE may be hampered by the formation of undesired byproducts or deactivation of the catalyst's active site due to the presence of water. This condition can be overcome by modifying the pore structure and acidity of the zeolite.<sup>21,22</sup>

Lately, modifications of zeolite have been thoroughly explored to enhance their properties with high conversion, desired selectivity, and yield, and in a particular process. Transition metal phosphates (MP) are currently attracting significant attention because of their simple preparation, excellent activity, and superior stability.<sup>23</sup> Various MP materials, such as nickel, cobalt, boron, and manganese phosphates, have been developed and are widely used in broad applications.<sup>24–28</sup> MP with tunable acid characteristics have been employed as catalysts for dehydration reactions because of their diverse structures and compositions.<sup>29</sup> MP with relatively strong P–O covalent bonds have proved to be chemically stable, and the MP framework structure allows the transition MP to provide abundant active sites and good conductivity.<sup>30,31</sup> In addition, materials that are nontoxic, naturally abundant, and have vast potential also make MP receive prominent attention.<sup>32,33</sup> In particular, nickel phosphate is a noteworthy chemical in inorganic chemistry that has been employed in various applications, including supercapacitors, photocatalysts, energy conversion, sensors, lithium batteries, and electrocatalytic reactions.<sup>34–37</sup> Nickel phosphate has several benefits, including high efficiency, outstanding environmental compatibility, a stable bifunctional catalyst, and a low cost.<sup>38</sup> Specifically, Ni significantly impacts electrochemical performance, while P influences the formation of a stable structure.<sup>39</sup> Hence, by combining natural zeolite with nickel phosphate could potentially enhance the catalytic activity toward isopropyl alcohol conversion by providing a synergetic active site that promotes high production and selectivity on DIPE. According to the literature review, until now, the modification of natural zeolite using nickel phosphate has not been reported previously, and its applicability for isopropyl alcohol conversion and DIPE production is limited.

In this present work, the natural zeolite was modified using nickel phosphate using a simple impregnation method. The effect of metal loading of zeolite–nickel phosphate on isopropyl alcohol conversion, DIPE yield, and selectivity will be evaluated. The catalytic activity of zeolite–nickel phosphate would be compared with the zeolite–nickel catalyst. The as-synthesis catalyst would be assessed using X-ray diffraction (XRD), Fourier transform infrared (FTIR), scanning electron microscopy–energy-dispersive X-ray spectroscopy (SEM–EDX), and N<sub>2</sub> physisorption. The acidity of the catalyst will be examined using the gravimetric method and FTIR–pyridine. The products of isopropyl alcohol dehydration would be analyzed using gas chromatography–mass spectrometry (GC–MS).

## RESULTS AND DISCUSSION

**Characterization of the Catalyst.** In this present study, unmodified zeolite, zeolite-Ni, and zeolite-Ni(H<sub>2</sub>PO<sub>4</sub>)<sub>2</sub> were characterized using XRD, FTIR, SEM–EDX, N<sub>2</sub> physisorption, and acidity of catalysts. Figure 1 depicts XRD diffractograms of

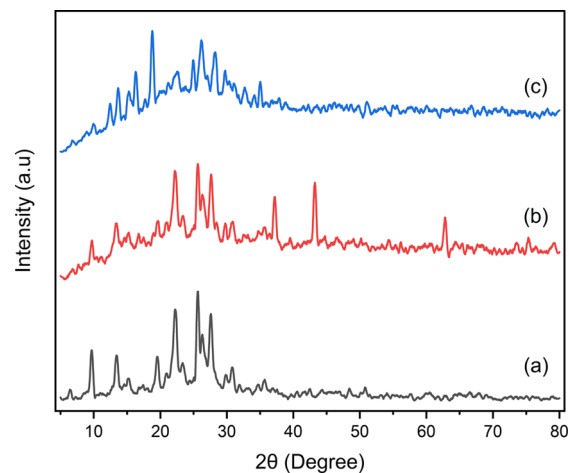


**Figure 1.** XRD diffractograms of (a) zeolite, (b) zeolite-Ni, (c) zeolite-Ni(H<sub>2</sub>PO<sub>4</sub>)<sub>2</sub>.

catalysts. It can be noticed that the diffraction peaks located at  $2\theta$  of 6.37°, 9.75°, 13.45°, 19.61°, 22.26°, 23.49°, 25.60°, 26.16°, 27.56°, and 29.77° in Figure 1a were ascribed as a type of the zeolite structure.<sup>40</sup> These typical peaks could be attributed to the mixture of clinoptilolite (JCPDS card 71-1425) as well as mordenite (JCPDS card 6-239) phases.<sup>41,42</sup> Yan et al.<sup>43</sup> and Wibowo et al.<sup>44</sup> also observed many mineral phases when preparing natural zeolite obtained from different districts. Subsequently, sharp peaks were spotted in the diffractograms, indicating that a crystalline phase catalyst had been acquired.<sup>45</sup> As presented in Figure 1b, a prominent peak at  $2\theta$  of 36.12°, 43.24°, 62.77°, 76.43°, and 78.12° appeared, which corresponded to the nickel oxide phase (JCPDS card 47-1049).<sup>46</sup> A distinguished diffractogram pattern of zeolite after being impregnated with nickel was also reported by Peron et al.<sup>47</sup> Moreover, the absence of the nickel oxide phase shown in Figure 1c indicated the new phase, that is, the Ni(H<sub>2</sub>PO<sub>4</sub>)<sub>2</sub> phase. This condition was confirmed as a new diffraction peak revealed at  $2\theta$  of 12.25°, 16.41°, 18.88°, 20°, 22.64°, 26.22°, 30.87°, and 33.12°, which corresponded to the nickel phosphate phase (JCPDS card 46-1388).<sup>48</sup> These peaks were relatively difficult to observe, presumably due to the highly dispersed Ni(H<sub>2</sub>PO<sub>4</sub>)<sub>2</sub> on the zeolite surface or the pore surface.<sup>49,50</sup> As presented in Figure 1, the main diffractogram of zeolite mineral remained unchanged after modifications, indicating that impregnation did not alter the crystalline zeolite structure.<sup>47</sup>

The morphological surface of catalysts at a magnification of 10,000 times is presented in Figure 2. The unmodified zeolite catalyst, as shown in Figure 2a, had a bulky structure with irregular plates. This appearance was consistently reported by Gea et al.<sup>51</sup> when preparing Sarulla natural zeolite and activated by acids. Another study also reported that natural zeolite had a granular structure.<sup>52</sup> Subsequently, Figure 2b shows that there was a relative change in the morphological surface of zeolite-Ni compared with unmodified zeolite. It was revealed that the nickel was dispersed toward the zeolite

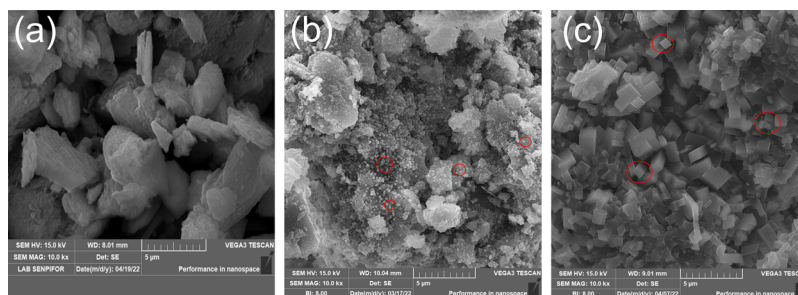


**Figure 2.** SEM micrographs of (a) zeolite, (b) zeolite-Ni, (c) zeolite-Ni(H<sub>2</sub>PO<sub>4</sub>)<sub>2</sub>.

surface, which suggested that the nickel had been successfully impregnated. A similar finding was reported by Azzolina-Jury et al.<sup>53</sup> when preparing as-synthesized USY/Ni and ZSM-11/Ni zeolites. Upasen et al.<sup>46</sup> corroborated that the tiny particles were attributed to the nickel-based dispersion on the surface of the zeolite. Furthermore, as presented in Figure 2c, the morphological surface of zeolite-Ni(H<sub>2</sub>PO<sub>4</sub>)<sub>2</sub> showed distinguishable morphologies from the zeolite–nickel, presumably due to the effect of phosphate species.

Chemical compositions of zeolite and modified zeolite analyzed by EDX are shown in Table 1. It can be seen that

**Table 1. Chemical Compositions of the Catalyst Analyzed by EDX**

elements	atomic (%)		
	zeolite	zeolite-Ni	zeolite-Ni(H <sub>2</sub> PO <sub>4</sub> ) <sub>2</sub>
O	55.16	60.24	68.07
Si	20.98	22.44	5.45
Al	4.97	4.24	1.1
Ni		10.59	4.05
P			20.68
C	15.88		
impurities	3.01	2.49	0.65

zeolite mainly contains oxygen, silica, and aluminum as a major constituent of the zeolite framework. A similar finding was coherently reported by Wibowo et al.<sup>44</sup> when preparing the natural zeolite from Suka Bumi, West Java. Because the as-prepared zeolite was collected from nature, 3.01% of impurities such as alkali and transition metals were reasonably detected. Low metal impurities were present on the zeolite, which was due to the activation by acid prior to modification.<sup>54</sup> Furthermore, 15.88% of carbon was detected in zeolite, and this condition was also reported by Gea et al.<sup>51</sup> which reported that Sarulla natural zeolite had a considerable amount of carbon (20.27–23.25%). According to Table 1, there was an increase in the nickel content up to 10.59%, which indicated that nickel had been successfully impregnated on the zeolite. A similar circumstance was also reported by Permata et al.<sup>55</sup> which showed that the nickel constituent was presented after introducing the nickel to the zeolite, as confirmed by EDX analysis. Moreover, the coexistence of 4.05% of nickel, 20.68% of phosphate, and 68.07% of oxygen presumably corresponded to the presence of nickel phosphate.<sup>37</sup> Table 1 also shows that the Si/Al ratio relatively remains unchanged, indicating that the zeolite structure was sustained during modifications.<sup>50</sup> The EDX analysis was consistent with XRD and SEM analyses, as previously described.

The functional groups of zeolite-Ni and zeolite-Ni(H<sub>2</sub>PO<sub>4</sub>)<sub>2</sub> are presented in Figure 3. The zeolite-Ni (Figure 3a) exhibited

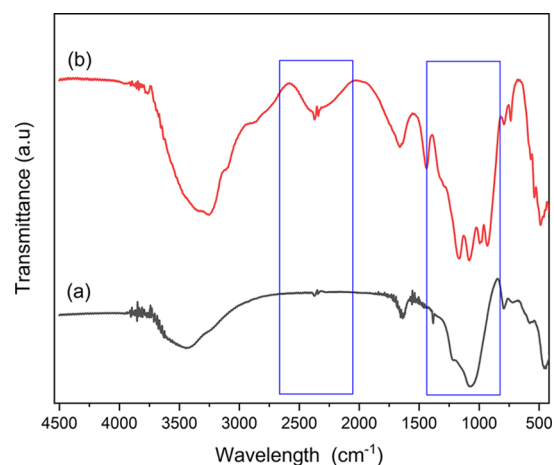


**Figure 3.** FTIR results of (a) zeolite-Ni and (b) zeolite-Ni(H<sub>2</sub>PO<sub>4</sub>)<sub>2</sub>.

peaks at 3620 cm<sup>-1</sup>, which were attributed to the stretching vibration of isolated OH groups from water that interacted with cations.<sup>56</sup> The bending vibration of H–O–H water or Si–OH molecules was also observed at 1670 cm<sup>-1</sup>.<sup>57</sup> The bands at 1076–1211 cm<sup>-1</sup> corresponded to the asymmetric strain vibrations of silicon–oxygen bonds (SiO<sub>4</sub>) as well as aluminum–oxygen (AlO<sub>4</sub>) in a tetrahedral network.<sup>44</sup> Subsequently, low intense bands at 457 and 794 cm<sup>-1</sup> were associated with the symmetrical strain vibrations of the O–Al–O and Si–O–Si bridge bonds.<sup>58</sup> On the other hand, the bending vibrations of Ni–O and Ni–O–H were observed at 453 and 558 cm<sup>-1</sup>, respectively.<sup>24,36</sup> These typical zeolite-Ni peaks, that is, zeolite frameworks and nickel functional groups, also appeared on the zeolite-Ni(H<sub>2</sub>PO<sub>4</sub>)<sub>2</sub> catalyst (Figure 3b) with a slight shift due to the interaction of hydrogen phosphate ions. As can be seen in Figure 3b, the apparent new peaks were clearly observed at 2335 cm<sup>-1</sup>, corresponding to the (P)–OH group vibration.<sup>59</sup> Furthermore, the peak at 763 cm<sup>-1</sup> was attributed to the vibration deformation of the P–O–P group,<sup>39,60</sup> whereas the peaks at 921, 983, and 1436 cm<sup>-1</sup> were assigned to the asymmetric bending vibrations of phosphate ions.<sup>24,31</sup> According to these results, the modification of zeolite using nickel and nickel phosphate was successfully accomplished.

Figure 4a shows the acidity value of natural zeolite, zeolite-Ni, and zeolite-Ni(H<sub>2</sub>PO<sub>4</sub>)<sub>2</sub> with various metal loadings calculated using the gravimetric method with pyridine as a probe. As shown in Figure 4a, natural zeolite had the lowest acid value (0.431 mmol of pyridine/g), whereas zeolite–nickel

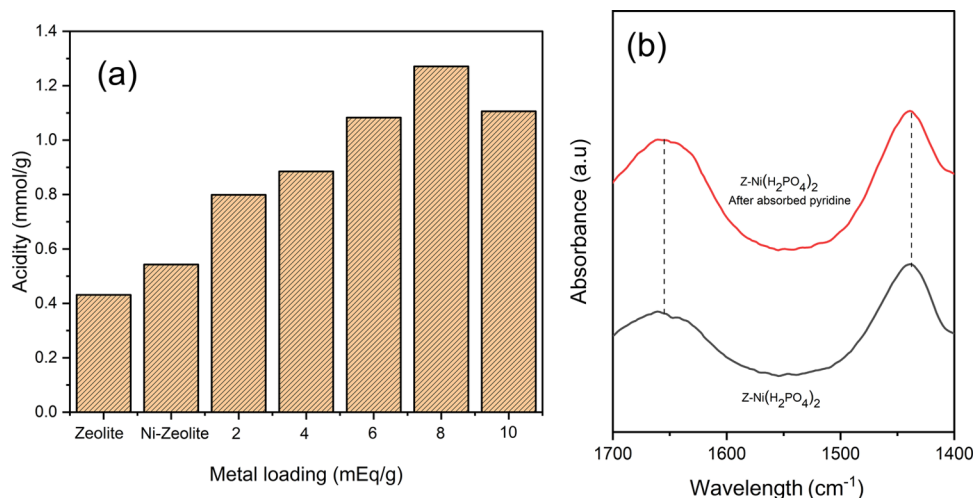


**Figure 4.** (a) Acidity analysis of natural zeolite, zeolite-Ni, and zeolite-Ni(H<sub>2</sub>PO<sub>4</sub>)<sub>2</sub> catalysts at various metal loadings. (b) FTIR spectra before and after pyridine was adsorbed.

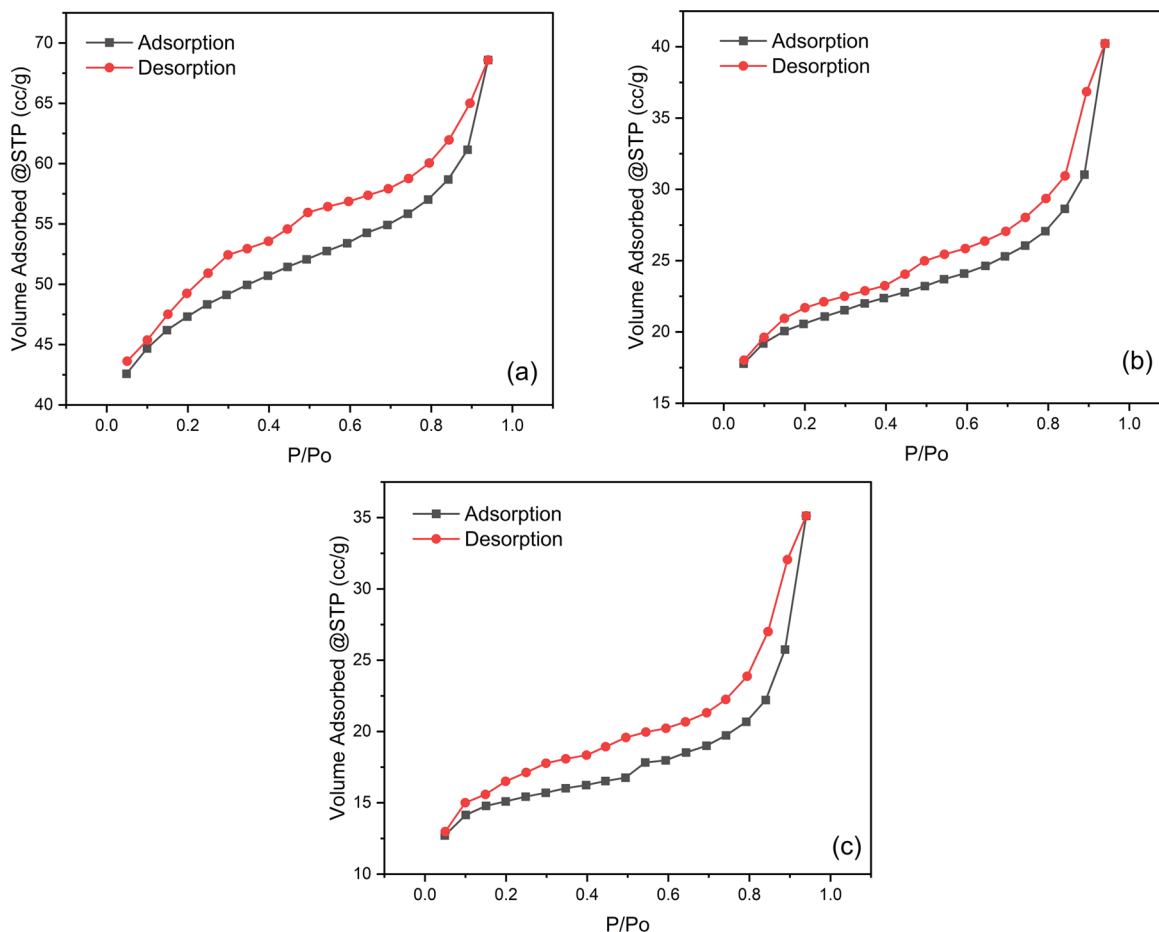


**Figure 5.** N<sub>2</sub> adsorption–desorption isotherms of (a) zeolite, (b) zeolite-Ni, and (c) zeolite-Ni(H<sub>2</sub>PO<sub>4</sub>)<sub>2</sub> catalysts.

contributed an acid value higher than that of natural zeolite (0.54 mmol of pyridine/g) because of weak acid sites of the aluminosilicate matrix<sup>61</sup> and impregnated nickel.<sup>55</sup> After modifications using nickel phosphate, at 2 mEq/g of metal loading, the acidity of zeolite–nickel increased up to 0.79 mmol of pyridine/g. This condition indicated that the presence of phosphate groups and their synergetic effect on metal, that is, nickel, presumably promoted the increase in acidity strongly

by introducing a new active site.<sup>59</sup> Furthermore, a prolonged metal loading to 8 mEq/g dramatically increases the acidity of the catalyst up to 1.27 mmol of pyridine/g. This condition was presumably associated with more acid sites presented in the zeolite-Ni(H<sub>2</sub>PO<sub>4</sub>)<sub>2</sub> catalyst.<sup>62</sup> However, higher metal loading (10 mEq/g) decreased the acidity of the catalyst to 1.106 mmol of pyridine/g, which might be due to the agglomeration of nickel phosphate on zeolite. A similar condition was

**Table 2. Textural Properties of Natural and Modified Zeolite**

catalyst	surface area (m <sup>2</sup> /g)	micropore area (m <sup>2</sup> /g)	external surface area (m <sup>2</sup> /g)	total pore volume (cc/g)	average pore size (nm)
zeolite	149.42	115.78	33.64	0.11	1.42
zeolite-Ni	65.57	46.74	18.83	0.06	1.90
zeolite-Ni(H <sub>2</sub> PO <sub>4</sub> ) <sub>2</sub>	46.95	33.03	13.92	0.05	2.27

reported by Susi et al.<sup>63</sup> when preparing zeolite loaded with nickel. The agglomeration made the acidity unevenly distributed; as a consequence, the adsorption of pyridine by the catalyst's active site was ineffective. Some studies have reported that agglomeration could reduce the catalyst acid sites as well.<sup>2,64</sup>

The FTIR spectra of zeolite-Ni(H<sub>2</sub>PO<sub>4</sub>)<sub>2</sub> before and after pyridine was adsorbed is presented in Figure 4b. Timofeeva et al.<sup>65</sup> stated that the evaluation of adsorbed bases through a spectroscopic study could be discerned between the Lewis and Brønsted acid sites. It can be seen that the intensity of both bands shown in Figure 4b increased after the catalyst adsorbed the pyridine molecule. The band at 1650 cm<sup>-1</sup> was attributed to the representative of pyridinium ions, which demonstrated the existence of Brønsted active sites from P(OH) groups,<sup>59</sup> whereas at 1430 cm<sup>-1</sup>, it was noticed due to the molecule of pyridine adsorbed to the Lewis acid sites.<sup>66,67</sup> These active sites inherently affect the dehydration process.<sup>68</sup>

The N<sub>2</sub> physisorption isotherms of natural zeolite, zeolite-Ni, and zeolite-Ni(H<sub>2</sub>PO<sub>4</sub>)<sub>2</sub> are shown in Figure 5. As can be seen in Figure 5, the zeolite and both modified zeolites had relatively similar N<sub>2</sub> adsorption–desorption isotherms which indicated that the structure zeolite was not altered by the modification of nickel and nickel phosphate.<sup>69</sup> Based on the IUPAC classification, those isotherms corresponded to type II isotherms. A similar finding was also reported by other studies when preparing natural zeolite.<sup>57</sup> The demonstration of a broad curve was observable, extending up to prolonged relative pressures, which was attributed to the typical wide mesoporosity and microporosity.<sup>70</sup> These isotherms had a hysteresis loop of the H4 type, which indicated the existence of the mesopore structure.<sup>71</sup> These hysteresis loops were frequently attributed to the narrow slitlike pores as well as particles with irregularly shaped internal cavities.<sup>72</sup> Regardless of the physisorption curve of all catalysts comparatively being the same, the relative alteration of the hysteresis loop of catalysts was presumably due to the effect of modification with changed pore content.<sup>73</sup>

The textural properties of natural and modified zeolite are elaborated in Table 2. According to Table 2, natural zeolite had a high surface area of 149.42 m<sup>2</sup>/g, which significantly decreased up to 56.11 and 68.58% after being impregnated with nickel and nickel phosphate species, respectively. The decrease in the zeolite surface area after being modified has been consistently reported in other studies.<sup>46,53,57,74,75</sup> This condition may be due to pore channel blocking of zeolite by nickel and nickel phosphate species.<sup>76</sup> The surface area of zeolite-Ni is 65.57 m<sup>2</sup>/g, which is higher than that of zeolite-Ni(H<sub>2</sub>PO<sub>4</sub>)<sub>2</sub>, which only had a surface area of 46.95 m<sup>2</sup>/g. Because the aggregate of nickel phosphate species was sufficiently bulk than nickel, this may lead the pores in or in the middle or center of the channel zeolite to be effectively blocked, thus leading zeolite-Ni(H<sub>2</sub>PO<sub>4</sub>)<sub>2</sub> to generate a low surface area than zeolite-Ni. This condition was also linear, with an increased average pore size of the modified zeolite, whereby the zeolite-Ni(H<sub>2</sub>PO<sub>4</sub>)<sub>2</sub> was higher than zeolite-Ni.

Moreover, as can be seen in Table 2, the total pore volume of parent zeolite also decreased after being modified, which was consistent with previous reports.<sup>61,75</sup> Furthermore, the micropore and external surface of parent zeolite were decreased after being modified, and this indicated that the nickel and nickel phosphate species were mostly located at both the micropore and external surface of the zeolite.<sup>49</sup>

**Conversion of Isopropyl Alcohol.** In this present study, 0.5 g of natural zeolite, zeolite-Ni, and zeolite-Ni(H<sub>2</sub>PO<sub>4</sub>)<sub>2</sub> were employed to catalyze the conversion of isopropyl alcohol (50 mL) under a reflux system at a mild reaction temperature of 150 °C for 3.5 h. The selectivity and yield of DIPE were also evaluated with various metal loadings of catalysts. Figure 6

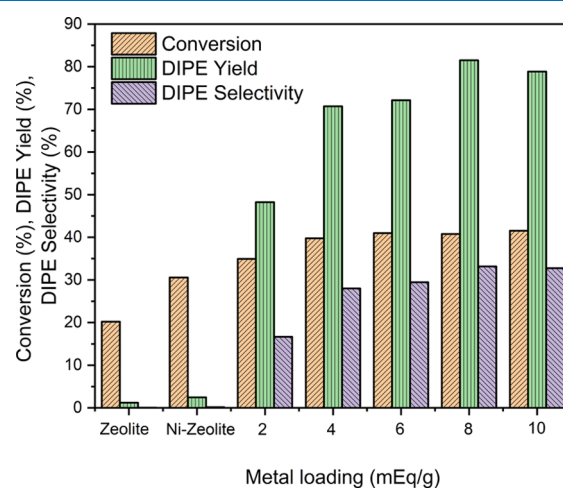


**Figure 6.** Catalytic activity of natural zeolite, zeolite-Ni, and zeolite-Ni(H<sub>2</sub>PO<sub>4</sub>)<sub>2</sub> at various metal loadings.

shows the catalytic activity of natural zeolite, zeolite-Ni, and zeolite-Ni(H<sub>2</sub>PO<sub>4</sub>)<sub>2</sub> toward isopropyl alcohol conversion, DIPE yield, and selectivity, respectively, at various catalyst metal loadings. As shown in Figure 6, natural zeolite generated 20.2% toward isopropyl alcohol conversion and increased to 30.57% when using a zeolite-Ni catalyst. Natural zeolite only had a low acidic site derived from zeolite's aluminosilicate matrix. This increase in isopropyl alcohol conversion was presumably due to the increase in the acidic site of the catalyst, which originated from Ni as a Lewis acid site.<sup>77</sup> The Ni species on natural zeolite promotes the catalytic activity toward isopropyl alcohol conversion. Furthermore, by employing 2 mEq/g of zeolite-Ni(H<sub>2</sub>PO<sub>4</sub>)<sub>2</sub>, the isopropyl alcohol conversion was increased 34.93%. The isopropyl alcohol conversion tended to increase up to 39.76% when the catalyst loading of 4 mEq/g zeolite-Ni(H<sub>2</sub>PO<sub>4</sub>)<sub>2</sub> was employed. The increase of isopropyl alcohol conversion by Ni(H<sub>2</sub>PO<sub>4</sub>)<sub>2</sub> suggested that the addition of phosphate ions into the catalyst affects the conversion due to high acidic active sites. Bedia et al.<sup>12</sup> stated that high acidic sites can be attributed to the high isopropyl alcohol conversion. Moreover, a prolonged catalyst loading above 4 mEq/g had an insignificant impact on the

isopropyl alcohol conversion, whereby the conversion likely tended to achieve equilibrium with a relatively constant isopropyl alcohol conversion ranging from 40.77–41.5%.

With regard to the DIPE yield, only 1.21 and 2.48% were achieved by a natural zeolite and zeolite-Ni catalyst, respectively. Surprisingly, a remarkable increase in DIPE yields up to 48.22% was noticed when employing zeolite-Ni( $\text{H}_2\text{PO}_4$ )<sub>2</sub> with 2 mEq/g catalyst loading. A similar condition was reported by Yaripour et al.<sup>78</sup> which showed that the phosphorous alumina catalyst showed higher catalytic activity compared with unmodified alumina. Moreover, a prolonged zeolite-Ni( $\text{H}_2\text{PO}_4$ )<sub>2</sub> metal loading increased the DIPE yield up to 81.51% at 8 mEq/g catalyst loading and a slightly decreased DIPE yield (78.58%) at 10 mEq/g catalyst loading. This trend was consistent with the catalyst acidity results and suggested that the catalytic activity behavior was robustly correlated to the acidic active sites. Armenta et al.<sup>7</sup> stated that the acidic site on the catalyst provided enormous hydrogen ions, which interact with isopropyl alcohol to generate high DIPE product. Isopropyl alcohol catalyzed by the Brønsted acid site was likely a typical acid–base reaction, which started with the formation of a protonated alcohol group and was followed by the attack of the nucleophile on the carbon atom and then replacing water molecules. The final DIPE product was generated through the deprotonation process. The catalyzing process of the dehydration reaction through Lewis acid was also favorable but required higher energy activation.<sup>7</sup>

Regarding the selectivity of DIPE, as shown in Figure 6, natural zeolite and zeolite-Ni had a low DIPE selectivity, which was only 0.05 and 0.16%, respectively. As the same trend with isopropyl alcohol conversion and DIPE yield, the DIPE selectivity remarkably enhanced to 16.68% after employing the zeolite-Ni( $\text{H}_2\text{PO}_4$ )<sub>2</sub> 2 mEq/g metal loading catalyst. The highest DIPE selectivity was achieved by 8 mEq/g metal loading zeolite-Ni( $\text{H}_2\text{PO}_4$ )<sub>2</sub> with 32.75% DIPE selectivity. More than 8 mEq/g metal loading generated a relatively constant DIPE selectivity, which was presumably due to the saturation of the catalyst's active site. This high selectivity toward DIPE was presumably derived from the synergetic Brønsted and Lewis acid sites derived from Ni–O–P centers.<sup>79</sup> Limlamthong et al.<sup>80</sup> reported that the introduction of the phosphorous species into alumina noticeably enhances the selectivity of diethyl ether. Some study reported that high DIPE selectivity might be correlated to the decrease in catalyst's surface area and type of pores;<sup>13,22</sup> however, despite the fact that this study also revealed the same, it was considered that acidity was a dominant factor over the surface area regarding DIPE selectivity. This proposed condition was also reported by Ni et al.<sup>59</sup> when employing zirconium phosphate for sorbitol and fructose dehydration, as well as by Armenta et al.<sup>7</sup> while using the supported iron oxide catalyst for 2-propanol dehydration. Turek et al.<sup>15</sup> reported that  $\gamma$ - $\text{Al}_2\text{O}_3$  and  $\text{ZrO}_2$  catalysts produced 8.6 and 0% toward diisopropyl ether selectivity, respectively, whereas heteropoly acids with various molar ratios produced 24–33.2%, under the temperature reaction of 206.85 °C. Min et al.<sup>17</sup> generated 5–13% of DIPE when employing  $\text{SiO}_2$ – $\text{ZrO}_2$  catalysts at 180–210 °C. Rekoske and Barteau<sup>81</sup> reported that high DIPE selectivity up to 100% was achieved using the  $\text{TiO}_2$  catalyst at a temperature of 175 °C, but the isopropyl alcohol conversion was only 6%.<sup>81</sup> According to Figure 6, the catalytic activity of zeolite-Ni( $\text{H}_2\text{PO}_4$ )<sub>2</sub> on isopropyl alcohol dehydration was relatively comparable with other catalysts. Despite the fact that

the zeolite-Ni( $\text{H}_2\text{PO}_4$ )<sub>2</sub> catalyst exhibited relatively high isopropyl conversion, further optimization of the dehydration process, such as temperature, reaction time, and other parameters, is necessary to be explored in order to get optimum results.

The reusability study of 8 mEq/g zeolite-Ni( $\text{H}_2\text{PO}_4$ )<sub>2</sub> catalyst was performed to see their stability toward isopropyl alcohol dehydration. This catalyst was employed because it exhibited the highest catalytic activity toward isopropyl alcohol dehydration. Figure 7 represents the catalyst reusability

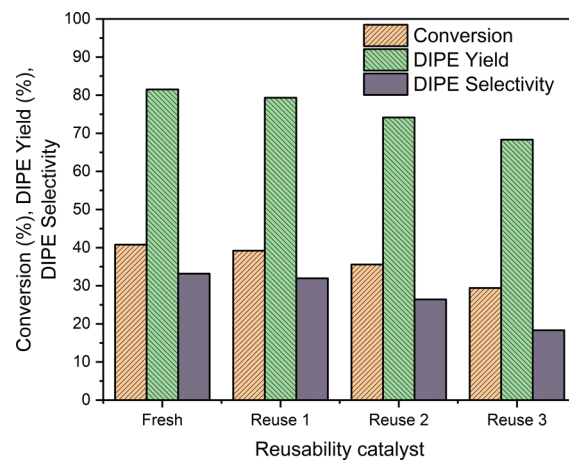


Figure 7. Reusability of the zeolite-Ni( $\text{H}_2\text{PO}_4$ )<sub>2</sub> catalyst.

performance at three consecutive runs. It can be seen that in the first cycle, isopropyl alcohol conversion decreased to 39.21%, whereas the DIPE yield and selectivity also decreased to 79.32 and 21.96%, respectively, which implied that there was a decrease in the catalytic performance to 2.79% on the isopropyl alcohol conversion, 3.82 and 3.61% on the DIPE yield and selectivity, respectively. Furthermore, the catalytic performance toward isopropyl alcohol dehydration gradually decreased in three consecutive runs. This issue was most likely caused by the leaching of the catalyst's active site during the regeneration process.<sup>82</sup> The reusability study suggested that the zeolite-Ni( $\text{H}_2\text{PO}_4$ )<sub>2</sub> catalyst was still active and had adequate catalytic activity stability toward isopropyl alcohol after the third cycle was reused.

## CONCLUSIONS

In this study, the modification of natural zeolite using nickel and nickel phosphate using the impregnation method was successfully accomplished, and the resulting catalyst enhanced the catalyst acidity and showed adequate catalytic activity in the conversion of isopropyl alcohol. The zeolite-Ni( $\text{H}_2\text{PO}_4$ )<sub>2</sub> had a cubic-like structure with higher acidity compared with zeolite-Ni. This high catalyst acidity with the existence of Brønsted and Lewis acid sites derived from nickel phosphate species was considered to significantly affect the catalytic activity toward isopropyl alcohol conversion. The study revealed that the highest catalytic activity toward isopropyl alcohol dehydration was achieved by the catalyst loading of 8 mEq/g zeolite-Ni( $\text{H}_2\text{PO}_4$ )<sub>2</sub> with isopropyl alcohol conversion of 40.77%, diisopropyl ether yield, and selectivity of 81.51 and 33.16%. The reusability study suggested that the zeolite-Ni( $\text{H}_2\text{PO}_4$ )<sub>2</sub> catalyst was still active and had sufficient catalytic activity stability toward isopropyl alcohol after the third cycle reused. This study suggested that the zeolite-Ni( $\text{H}_2\text{PO}_4$ )<sub>2</sub> had

adequate performance and potential as an acceptable choice for upscale isopropyl alcohol conversion. Further optimization conversion study was necessary to improve the output process.

## MATERIALS AND METHODS

**Preparation of Zeolite.** A bulky natural zeolite (Bayan, West Java) was sieved up to 200-mesh and dried in an oven at 120 °C for 3 h. The zeolite was activated prior to modification using 1% HF solution by stirring for 1 h and subsequently washed with distilled water. Afterward, the zeolite was saturated with 6 N HCl for 4 h. The zeolite was filtered and washed using distilled water until the pH gradually reached neutral. Lastly, the zeolite was dried in the oven at 120 °C for 12 h.

**Modification of Zeolite.** The zeolite modification was conducted using the impregnation method. Briefly, 0.1 M Ni(NO<sub>3</sub>)<sub>2</sub>·6H<sub>2</sub>O solution as the Ni<sup>2+</sup> precursor, with different metal loadings of 2, 4, 6, 8, and 10 mEq/g, was mixed with 1 M NH<sub>4</sub>H<sub>2</sub>PO<sub>4</sub> solution and 5 g of activated zeolite. The mixture was stirred for 24 h at room temperature. Afterward, while stirring, the temperature gradually increased up to 80 °C until the paste formed and dried in the oven at 105 °C. The powder was later calcined at 350 °C for 4 h. The modified zeolite was referred to as the zeolite-Ni(H<sub>2</sub>PO<sub>4</sub>)<sub>2</sub> catalyst. As a comparison, the zeolite-Ni catalyst was also prepared with the same procedure without adding phosphate solution.

**Study of Isopropyl Alcohol Dehydration.** Dehydration of isopropyl alcohol was conducted in a batch reactor using 0.5 g of catalyst and 50 mL of isopropanol alcohol at 150 °C for 3.5 h. The product was separated with the catalyst and analyzed using GC–MS. The isopropyl alcohol conversion ( $X_{\text{conversion}}$ ), diisopropyl ether yield ( $Y_{\text{yield}}$ ), and selectivity ( $Y_{\text{selectivity}}$ ) were evaluated according to eqs 123, respectively, as follows:

$$X_{\text{conversion}} = \frac{n_o - n}{n_o} \times 100 \quad (1)$$

$$Y_{\text{yield}} = \frac{y \times 2}{n_o - n} \times 100 \quad (2)$$

$$Y_{\text{selectivity}} = \frac{y}{n_o} \times 100 \quad (3)$$


where  $n_o$  and  $n$  are the initial and final mole of isopropyl alcohol, whereas  $y$  is the mole product of diisopropyl ether.

**Characterization of the Catalyst.** Rigaku MiniFlex 600 (Cu-K $\alpha$  rays with a wavelength of 1.5406 Å) was employed to measure the crystal structure of catalysts. FTIR Shimadzu-Prestige 21 was used to determine the functional groups of catalysts. The acidity of the catalyst was examined using the gravimetric method with pyridine gas as a probe,<sup>2</sup> and the FTIR-adsorbed pyridine was also analyzed. Tescan Vega 3 SEM with EDX was assessed to determine the morphology and the elemental composition of the catalyst. The textural characteristics of catalysts were analyzed using Quantachrome NOVA.

## AUTHOR INFORMATION

### Corresponding Author

Hasanudin Hasanudin – Department of Chemistry, Faculty of Mathematics and Natural Science and Biofuel Research Group, Faculty of Mathematics and Natural Science, Universitas Sriwijaya, Palembang, Sumatra Selatan 30662,

Indonesia;  [orcid.org/0000-0003-2153-9163](https://orcid.org/0000-0003-2153-9163);  
Phone: +6281367471272; Email: [hasanudin@mipa.unsri.ac.id](mailto:hasanudin@mipa.unsri.ac.id)

## Authors

Wan Ryan Asri – Department of Chemistry, Faculty of Mathematics and Natural Science and Biofuel Research Group, Faculty of Mathematics and Natural Science, Universitas Sriwijaya, Palembang, Sumatra Selatan 30662, Indonesia

Lola Andini – Department of Chemistry, Faculty of Mathematics and Natural Science and Biofuel Research Group, Faculty of Mathematics and Natural Science, Universitas Sriwijaya, Palembang, Sumatra Selatan 30662, Indonesia

Fahma Riyanti – Department of Chemistry, Faculty of Mathematics and Natural Science and Biofuel Research Group, Faculty of Mathematics and Natural Science, Universitas Sriwijaya, Palembang, Sumatra Selatan 30662, Indonesia

Ady Mara – Department of Chemistry, Faculty of Mathematics and Natural Science and Biofuel Research Group, Faculty of Mathematics and Natural Science, Universitas Sriwijaya, Palembang, Sumatra Selatan 30662, Indonesia

Fitri Hadiah – Department of Chemical Engineering, Faculty of Engineering, Universitas Sriwijaya, Palembang, Sumatra Selatan 30662, Indonesia

Zainal Fanani – Department of Chemistry, Faculty of Mathematics and Natural Science and Biofuel Research Group, Faculty of Mathematics and Natural Science, Universitas Sriwijaya, Palembang, Sumatra Selatan 30662, Indonesia

Complete contact information is available at:

<https://pubs.acs.org/10.1021/acsomega.2c04647>

## Notes

The authors declare no competing financial interest.

## ACKNOWLEDGMENTS

The authors thank Biofuel Research Group, the Faculty of Mathematics and Natural Science, Universitas Sriwijaya, for the collaborative work and for facilitating this research. We also acknowledge the National Research and Innovation Agency (Badan Riset dan Inovasi Nasional) for providing access to instrumental analysis.

## REFERENCES

- (1) Kashyap, P.; Gahlyan, S.; Rani, M.; Tiwari, D. P.; Maken, S. Thermophysical Properties of Ternary Liquid Mixture of Diisopropyl Ether (1) + Ethanol (2) + n-Heptane (3): Measurement and Correlation. *J. Mol. Liq.* **2020**, *319*, No. 114219.
- (2) Hasanudin, H.; Asri, W. R.; Tampubolon, K.; Riyant, F.; Purwaningrum, W.; Wijaya, K. Dehydration Isopropyl Alcohol to Diisopropyl Ether over Molybdenum Phosphide Pillared Bentonite. *Pertanika J. Sci. Technol.* **2022**, *30*, 1739–1754.
- (3) Muñoz-Rujas, N.; Bazile, J. P.; Aguilar, F.; Galliero, G.; Montero, E.; Daridon, J. L. Speed of Sound, Density and Derivative Properties of Diisopropyl Ether under High Pressure. *Fluid Phase Equilib.* **2017**, *449*, 148–155.
- (4) Fan, X.; Sun, W.; Liu, Z.; Gao, Y.; Yang, J.; Yang, B.; Law, C. K. Exploring the Oxidation Chemistry of Diisopropyl Ether: Jet-Stirred Reactor Experiments and Kinetic Modeling. *Proc. Combust. Inst.* **2021**, *38*, 321–328.

- (5) Ahmadi, S.; Almasi, M. Experimental and Modeling Study of Diisopropyl Ether and 2-Alkanol; PC-SAFT Model and Free Volume Theory. *J. Chem. Thermodyn.* **2020**, *142*, No. 106025.
- (6) Heese, F. P.; Dry, M. E.; Möller, K. P. The Mechanism of Diisopropyl Ether Synthesis from a Feed of Propylene and Isopropanol over Ion Exchange Resin. *Stud. Surf. Sci. Catal.* **2000**, *130 C*, 2597–2602.
- (7) Armenta, M. A.; Valdez, R.; Silva-Rodrigo, R.; Olivas, A. Diisopropyl Ether Production via 2-Propanol Dehydration Using Supported Iron Oxides Catalysts. *Fuel* **2019**, *236*, 934–941.
- (8) Wang, C.; Jia, M.; Bai, Z.; Shi, M.; Chen, X.; Fan, J.; Dai, F. The Separation of Isopropyl Alcohol from Diisopropyl Ether System Using Glycols: Phase Equilibrium and Rigorous Correlation. *J. Chem. Thermodyn.* **2020**, *150*, No. 106230.
- (9) Chidambaram, V.; Viswanathan, B. Single Step Catalytic Production of Diisopropyl Ether (DIPE) from Acetone Feedstock over Nickel Based Catalysts. *Appl. Catal., B* **2007**, *71*, 32–43.
- (10) Uyumaz, A.; Aydoğan, B.; Calam, A.; Aksoy, F.; Yılmaz, E. The Effects of Diisopropyl Ether on Combustion, Performance, Emissions and Operating Range in a HCCI Engine. *Fuel* **2020**, *265*, No. 116919.
- (11) Cheng, Z.; Wang, H.; Yin, W.; Wang, J.; Li, W.; Wang, Z.; Xing, L.; Gao, X.; Mei, B.; Zhang, Y.; Yang, J.; Wei, L.; Zhong, X.; Wang, H.; Li, Y.; Yan, B.; Chen, G. Experimental and Kinetic Modeling Study of Di-n-Propyl Ether and Diisopropyl Ether Combustion: Pyrolysis and Laminar Flame Propagation Velocity. *Combust. Flame* **2022**, *237*, No. 111809.
- (12) Bedia, J.; Ruiz-Rosas, R.; Rodríguez-Mirasol, J.; Cordero, T. A Kinetic Study of 2-Propanol Dehydration on Carbon Acid Catalysts. *J. Catal.* **2010**, *271*, 33–42.
- (13) Morales-Anzures, F.; Salinas-Hernández, P.; Ornelas-Gutiérrez, C.; Tzompantzi-Morales, F. J.; Pérez-Hernández, R. Synthesis by the Sol-Gel Method and Characterization of Pt-Promoted CuO/TiO<sub>2</sub>-ZrO<sub>2</sub> Catalysts for Decomposition of 2-Propanol. *Catal. Today* **2020**, *349*, 228–234.
- (14) Benyounes, A.; Kacimi, M.; Ziyad, M.; Serp, P. Conversion of Isopropyl Alcohol over Ru and Pd Loaded N-Doped Carbon Nanotubes. *Chin. J. Catal.* **2014**, *35*, 970–978.
- (15) Turek, W.; Haber, J.; Krowiak, A. Dehydration of Isopropyl Alcohol Used as an Indicator of the Type and Strength of Catalyst Acid Centres. *Appl. Surf. Sci.* **2005**, *252*, 823–827.
- (16) Escobar, J.; De Los Reyes, J. A.; Viveros, T.; Valle-Orta, M.; Barrera, M. C. Compensation in the Isopropyl Alcohol Dehydration over Sol-Gel Al<sub>2</sub>O<sub>3</sub>-TiO<sub>2</sub> Oxides: Effect of Calcining Temperature. *Fuel* **2015**, *149*, 109–117.
- (17) Min, H. K.; Kim, Y. W.; Kim, C.; Ibrahim, I. A. M.; Han, J. W.; Suh, Y. W.; Jung, K. D.; Park, M. B.; Shin, C. H. Phase Transformation of ZrO<sub>2</sub> by Si Incorporation and Catalytic Activity for Isopropyl Alcohol Dehydration and Dehydrogenation. *Chem. Eng. J.* **2022**, *428*, No. 131766.
- (18) Gómez-Gutiérrez, C. M.; Luque, P. A.; Guerra-Rivas, G.; López-Sánchez, J. A.; Armenta, M. A.; Quintana, J. M.; Olivas, A. Solvothermal Synthesis of Nickel-Tungsten Sulfides for 2-Propanol Dehydration. *Scanning* **2015**, *37*, 165–171.
- (19) Tang, X.; Bumüller, D.; Lim, A.; Schneider, J.; Heiz, U.; Ganteför, G.; Fairbrother, D. H.; Bowen, K. H. Catalytic Dehydration of 2-Propanol by Size-Selected (WO<sub>3</sub>)<sub>n</sub> and (MoO<sub>3</sub>)<sub>n</sub> Metal Oxide Clusters. *J. Phys. Chem. C* **2014**, *118*, 29278–29286.
- (20) Masih, D.; Rohani, S.; Kondo, J. N.; Tatsumi, T. Low-Temperature Methanol Dehydration to Dimethyl Ether over Various Small-Pore Zeolites. *Appl. Catal., B* **2017**, *217*, 247–255.
- (21) Catizzone, E.; Aloise, A.; Migliori, M.; Giordano, G. Dimethyl Ether Synthesis via Methanol Dehydration: Effect of Zeolite Structure. *Appl. Catal., A* **2015**, *502*, 215–220.
- (22) Rutkowska, M.; Macina, D.; Mirocha-Kubień, N.; Piwowarska, Z.; Chmielarz, L. Hierarchically Structured ZSM-5 Obtained by Desilication as New Catalyst for DME Synthesis from Methanol. *Appl. Catal., B* **2015**, *174*, 336–343.
- (23) Zhang, X.; Sun, G.; Jia, S.; Xie, H.; Kang, Z.; Chen, W.; Cui, M.; Wang, B.; Wang, B.; Chen, X.; Yang, D. P. Intrinsic Carbon Defects Induced Nickel Phosphate/Carbon Photocatalyst for High Performance Bacterial Disinfection. *Chem. Eng. J.* **2022**, *438*, No. 135624.
- (24) Song, X.; Gao, L.; Li, Y.; Chen, W.; Mao, L.; Yang, J. H. Nickel Phosphate-Based Materials with Excellent Durability for Urea Electro-Oxidation. *Electrochim. Acta* **2017**, *251*, 284–292.
- (25) Sharma, P.; Radhakrishnan, S.; Khil, M. S.; Kim, H. Y.; Kim, B. S. Simple Room Temperature Synthesis of Porous Nickel Phosphate Foams for Electrocatalytic Ethanol Oxidation. *J. Electroanal. Chem.* **2018**, *808*, 236–244.
- (26) Song, X.; Sun, Q.; Gao, L.; Chen, W.; Wu, Y.; Li, Y.; Mao, L.; Yang, J. H. Nickel Phosphate as Advanced Promising Electrochemical Catalyst for the Electro-Oxidation of Methanol. *Int. J. Hydrogen Energy* **2018**, *43*, 12091–12102.
- (27) Wang, Z.; Chen, F.; Kannan, P.; Ji, S.; Wang, H. Nickel Phosphate Nanowires Directly Grown on Ni Foam as Binder-Free Electrode for Pseudocapacitors. *Mater. Lett.* **2019**, *257*, No. 126742.
- (28) Touny, A. H.; Abd El-Lateef, H. M.; Saleh, M. M. Removal of Cationic Surfactants from Dilute Solutions Using Nanoporous Nickel Phosphate: A Structural, Kinetic and Thermodynamic Study. *J. Mol. Liq.* **2019**, *283*, 30–38.
- (29) Otomo, R.; Yamaguchi, C.; Iwaisako, D.; Oyamada, S.; Kamiya, Y. Selective Dehydration of 1,2-Propanediol to Propanal over Boron Phosphate Catalyst in the Presence of Steam. *ACS Sustainable Chem. Eng.* **2019**, *7*, 3027–3033.
- (30) Ma, X.; Chen, J.; Yuan, B.; Li, Y.; Yu, L.; Zhao, W. Three-Dimensional Hollow Nickel Phosphate Microspheres with Controllable Hoya-like Structure for High-Performance Enzymeless Glucose Detection and Supercapacitor. *Appl. Surf. Sci.* **2022**, *588*, No. 152928.
- (31) Wulan Septiani, N. L.; Kaneti, Y. V.; Fathoni, K. B.; Wang, J.; Ide, Y.; Yulianto, B.; Nugraha; Dipojono, H. K.; Nanjundan, A. K.; Golberg, D.; Bando, Y.; Yamauchi, Y. Self-Assembly of Nickel Phosphate-Based Nanotubes into Two-Dimensional Crumpled Sheet-like Architectures for High-Performance Asymmetric Supercapacitors. *Nano Energy* **2020**, *67*, No. 104270.
- (32) Arunachalam, P.; AlOraij, H. A.; Amer, M. S.; Hezam, M.; Shaddad, M. N.; Madhavan, J. Activation Effect of Nickel Phosphate Co-Catalysts on the Photoelectrochemical Water Oxidation Performance of TiO<sub>2</sub> Nanotubes. *J. Saudi Chem. Soc.* **2022**, *26*, No. 101484.
- (33) Li, N.; Xu, Z.; Liu, Y.; Hu, Z. Fructose 1,6-Bisphosphate Trisodium Salt as a New Organic Phosphorus Source for Synthesis of Nanoporous Amorphous Nickel Phosphate Microspheres Electrode Materials in Supercapacitors. *J. Alloys Compd.* **2019**, *789*, 613–621.
- (34) Xiao, L.; Yang, K.; Duan, J.; Zheng, S.; Jiang, J. The Nickel Phosphate Rods Derived from Ni-MOF with Enhanced Electrochemical Activity for Non-Enzymatic Glucose Sensing. *Talanta* **2022**, *247*, No. 123587.
- (35) Lee, S. K.; Lee, U. H.; Hwang, Y. K.; Chang, J. S.; Han Jang, N. Catalytic and Sorption Applications of Porous Nickel Phosphate Materials. *Catal. Today* **2019**, *324*, 154–166.
- (36) Kokulnathan, T.; Manikandan, R.; Chen, S. M.; Ponnusamy, V. K. Synthesis and Characterization of Nanostructured Nickel Phosphate as a Robust Electrocatalyst for the Highly Sensitive Voltammetric Determination of Chlorpromazine in Biological Sample. *J. Taiwan Inst. Chem. Eng.* **2018**, *93*, 11–20.
- (37) Al-Jendan, S. A.; Alarjan, W.; Elghamry, I.; Touny, A.; Saleh, M. M.; Abdelsalam, M. E. An Optimized Nickel Phosphate/Carbon Composite Electrocatalyst for the Oxidation of Formaldehyde. *Int. J. Hydrogen Energy* **2020**, *45*, 14320–14333.
- (38) Zhang, H.; Li, Z.; Hou, Z.; Mei, H.; Feng, Y.; Xu, B.; Sun, D. Self-Assembly of MOF on MXene Nanosheets and in-Situ Conversion into Superior Nickel Phosphates/MXene Battery-Type Electrode. *Chem. Eng. J.* **2021**, *425*, No. 130602.
- (39) Khalaf, M. M.; Abd El-Lateef, H. M.; Touny, A. H.; Saleh, M. M.; Mohamed, I. M. A. Electrocatalytic Performance of Inorganic Nanoflakes Nickel Phosphates under Adjusted Synthetic Parameters towards Urea and Methanol Oxidation in Alkaline Media. *Microchem. J.* **2021**, *163*, No. 105901.



- (40) Fereidooni, L.; Mehrpooya, M. Experimental Assessment of Electrolysis Method in Production of Biodiesel from Waste Cooking Oil Using Zeolite/Chitosan Catalyst with a Focus on Waste Biorefinery. *Energy Convers. Manage.* **2017**, *147*, 145–154.
- (41) Moradi, G. R.; Yaripour, F.; Vale-Sheyda, P. Catalytic Dehydration of Methanol to Dimethyl Ether over Mordenite Catalysts. *Fuel Process. Technol.* **2010**, *91*, 461–468.
- (42) Nodehi, R.; Shayesteh, H.; Kelishami, A. R. Enhanced Adsorption of Congo Red Using Cationic Surfactant Functionalized Zeolite Particles. *Microchem. J.* **2020**, *153*, No. 104281.
- (43) Yan, P.; Kennedy, E.; Stockenhuber, M. Natural Zeolite Supported Ni Catalysts for Hydrodeoxygenation of Anisole. *Green Chem.* **2021**, *23*, 4673–4684.
- (44) Wibowo, E.; Rokhmat, M.; Sutisna; Murniati, R.; Khairurrijal; Abdullah, M. Identification of Natural Zeolite from Sukabumi, West Java, Indonesia: Structure, Chemical Composition, Morphology and Molecular Vibration. *Mater. Res. Express* **2017**, *4*, No. 064002.
- (45) Fa, D.; Yu, B.; Miao, Y. Synthesis of Ultra-Long Nanowires of Nickel Phosphate by a Template-Free Hydrothermal Method for Electrocatalytic Oxidation of Glucose. *Colloids Surf., A* **2019**, *564*, 31–38.
- (46) Upasen, S.; Sarunchot, G.; Srira-ngam, N.; Poo-arporn, Y.; Wattanachai, P.; Prasertdam, P.; Ngaotranwiwat, P.; Panpranot, J.; Soisuwan, S. What If Zeolite LTA4A and Zeolite LTA5A Used as Nickel Catalyst Supports for Recycling Carbon Dioxide to Green Fuel Methane. *J. CO<sub>2</sub> Util.* **2022**, *55*, No. 101803.
- (47) Peron, D. V.; Zhobolobenko, V. L.; de la Rocha, M. R.; Oberson de Souza, M.; Feris, L. A.; Marcilio, N. R.; Ordonsky, V. V.; Khodakov, A. Y. Nickel–Zeolite Composite Catalysts with Metal Nanoparticles Selectively Encapsulated in the Zeolite Micropores. *J. Mater. Sci.* **2019**, *54*, 5399–5411.
- (48) Li, N.; Xu, Z.; Liu, Y.; Hu, Z. Hollow Amorphous Microspheres of Nickel Phosphate: Synthesis Using Adenosine 5'-Triphosphate Disodium Salt as a New Organic Phosphorus Source and Their Application as Electrode Materials in Supercapacitors. *J. Power Sources* **2019**, *426*, 1–10.
- (49) Kweon, S.; Kim, Y. W.; Bae, J.; Kim, E. J.; Park, M. B.; Min, H. K. Nickel on Two-Dimensional ITQ-2 Zeolite as a Highly Active Catalyst for Carbon Dioxide Reforming of Methane. *J. CO<sub>2</sub> Util.* **2022**, *58*, No. 101921.
- (50) Wei, L.; Kumar, N.; Haije, W.; Peltonen, J.; Peurla, M.; Grenman, H.; de Jong, W. Can Bi-Functional Nickel Modified 13X and 5A Zeolite Catalysts for CO<sub>2</sub> Methanation Be Improved by Introducing Ruthenium? *Mol. Catal.* **2020**, *494*, No. 111115.
- (51) Gea, S.; Haryono, A.; Andriyani, A.; Sihombing, J. L.; Pulungan, A. N.; Nasution, T.; Rahayu, R.; Hutapea, Y. A. The Stabilization of Liquid Smoke through Hydrodeoxygenation over Nickel Catalyst Loaded on Sarulla Natural Zeolite. *Appl. Sci.* **2020**, *10*, 4126.
- (52) Hasanudin, H.; Putri, Q. U.; Agustina, T. E.; Hadiah, F. Esterification of Free Fatty Acid in Palm Oil Mill Effluent Using Sulfated Carbon-Zeolite Composite Catalyst. *Pertanika. J. Sci. Technol.* **2022**, *30*, 377–395.
- (53) Azzolina-Jury, F.; Bento, D.; Henriques, C.; Thibault-Starzyk, F. Chemical Engineering Aspects of Plasma-Assisted CO<sub>2</sub> Hydrogenation over Nickel Zeolites under Partial Vacuum. *J. CO<sub>2</sub> Util.* **2017**, *22*, 97–109.
- (54) Adriano, A.; Cornejo, M. H.; Baykara, H.; Ludeña, E. V.; Brito, J. L. Dealumination and Characterization of Natural Mordenite-Rich Tuffs. *Materials* **2022**, *15*, 4654.
- (55) Permata, M. L.; Trisunaryanti, W.; Falah, I. I.; Hapsari, M. T.; Fatmawati, D. A. The Effect of Nickel Content Impregnated on Zeolite toward Catalytic Activity and Selectivity for Hydrotreating of Cashew Nut Shell Liquid Oil. *Rasayan J. Chem.* **2020**, *13*, 772–779.
- (56) Mansouri, N.; Rikhtegar, N.; Ahmad Panahi, H.; Atabi, F.; Shahraki, B. K. Porosity, Characterization and Structural Properties of Natural Zeolite-Clinoptilolite-As a Sorbent. *Environ. Prot. Eng.* **2013**, *39*, 139–152.
- (57) Sakizci, M.; Özgül Tanriverdi, L. Influence of Acid and Heavy Metal Cation Exchange Treatments on Methane Adsorption Properties of Mordenite. *Turkish J. Chem.* **2015**, *39*, 970–983.
- (58) Ba Mohammed, B.; Yamni, K.; Tijani, N.; Lee, H. S.; Dehmani, Y.; El Hamdani, H.; Alrashdi, A. A.; Ramola, S.; Belwal, T.; Lgaz, H. Enhanced Removal Efficiency of NaY Zeolite toward Phenol from Aqueous Solution by Modification with Nickel (Ni-NaY). *J. Saudi Chem. Soc.* **2021**, *25*, No. 101224.
- (59) Ni, W.; Li, D.; Zhao, X.; Ma, W.; Kong, K.; Gu, Q.; Chen, M.; Hou, Z. Catalytic Dehydration of Sorbitol and Fructose by Acid-Modified Zirconium Phosphate. *Catal. Today* **2010**, *2019*, 66–75.
- (60) Vinothkumar, V.; Sakthivel, R.; Chen, S. M.; Kim, T. H.; Abinaya, M.; Kubendhiran, S.; Gopu, G. Nanoarchitected Nickel Phosphate Integrated with Graphene Oxide for the Toxicant Diphenylamine Detection in Food Samples. *J. Food Compos. Anal.* **2022**, *111*, No. 104628.
- (61) Lee, C. W.; Lin, P. Y.; Chen, B. H.; Kukushkin, R. G.; Yakovlev, V. A. Hydrodeoxygenation of Palmitic Acid over Zeolite-Supported Nickel Catalysts. *Catal. Today* **2021**, *379*, 124–131.
- (62) Hasanudin, H.; Asri, W. R.; Said, M.; Hidayati, P. T.; Purwaningrum, W.; Novia, N.; Wijaya, K. Hydrocracking Optimization of Palm Oil to Bio-Gasoline and Bio-Aviation Fuels Using Molybdenum Nitride-Bentonite Catalyst. *RSC Adv.* **2022**, *12*, 16431–16443.
- (63) Susi, E. P.; Wijaya, K.; Wangsa; Pratika, R. A.; Hariani, P. L. Effect of Nickel Concentration in Natural Zeolite as Catalyst in Hydrocracking Process of Used Cooking Oil. *Asian J. Chem.* **2020**, *32*, 2773–2777.
- (64) Argyle, M. D.; Bartholomew, C. H. Heterogeneous Catalyst Deactivation and Regeneration: A Review. *Catalysts* **2015**, *5*, 145–269.
- (65) Timofeeva, M. N.; Panchenko, V. N.; Hasan, Z.; Jhung, S. H. Catalytic Potential of the Wonderful Chameleons: Nickel Phosphate Molecular Sieves. *Appl. Catal., A* **2013**, *455*, 71–85.
- (66) Sinhamahapatra, A.; Sutradhar, N.; Roy, B.; Tarafdar, A.; Bajaj, H. C.; Panda, A. B. Mesoporous Zirconium Phosphate Catalyzed Reactions: Synthesis of Industrially Important Chemicals in Solvent-Free Conditions. *Appl. Catal., A* **2010**, *385*, 22–30.
- (67) Bokade, V.; Moondra, H.; Niphadkar, P. Highly Active Brønsted Acidic Silicon Phosphate Catalyst for Direct Conversion of Glucose to Levulinic Acid in MIBK–Water Biphasic System. *SN Appl. Sci.* **2019**, *2*, 51.
- (68) Sarve, D. T.; Singh, S. K.; Ekhe, J. D. Ethanol Dehydration to Diethyl Ether over ZSM-5 and  $\beta$ -Zeolite Supported Ni–W Catalyst. *Inorg. Chem. Commun.* **2022**, *139*, No. 109397.
- (69) Alalga, L.; Benamar, A.; Trari, M. Hydrogen Production via Methane Decomposition over Nickel Supported on Synthesized ZSM-5/MCM-41 Zeolite Composite Material. *Int. J. Hydrogen Energy* **2021**, *46*, 28501–28512.
- (70) Palomo, J.; Rodríguez-Mirasol, J.; Cordero, T. Methanol Dehydration to Dimethyl Ether on Zr-Loaded P-Containing Mesoporous Activated Carbon Catalysts. *Materials* **2019**, *12*, 2204.
- (71) Chen, C.; Cai, L.; Zhang, L.; Fu, W.; Hong, Y.; Gao, X.; Jiang, Y.; Li, L.; Yan, X.; Wu, G. Transesterification of Rice Bran Oil to Biodiesel Using Mesoporous NaBeta Zeolite-Supported Molybdenum Catalyst: Experimental and Kinetic Studies. *Chem. Eng. J.* **2020**, *382*, No. 122839.
- (72) Ketzer, F.; Celante, D.; de Castilhos, F. Catalytic Performance and Ultrasonic-Assisted Impregnation Effects on WO<sub>3</sub>/USY Zeolites in Esterification of Oleic Acid with Methyl Acetate. *Microporous Mesoporous Mater.* **2020**, *291*, No. 109704.
- (73) Kazakov, M. O.; Nadeina, K. A.; Danilova, I. G.; Dik, P. P.; Klimov, O. V.; Pereyma, V. Y.; Gerasimov, E. Y.; Dobryakova, I. V.; Knyazeva, E. E.; Ivanova, I. I.; Noskov, A. S. Hydrocracking of vacuum gas oil over NiMo/Y-Al<sub>2</sub>O<sub>3</sub>: Effect of Mesoporosity Introduced by Zeolite Y Recrystallization. *Catal. Today* **2018**, *305*, 117–125.
- (74) Wei, L.; Haije, W.; Kumar, N.; Peltonen, J.; Peurla, M.; Grenman, H.; de Jong, W. Influence of nickel precursors on the

properties and performance of Ni impregnated zeolite 5A and 13X catalysts in CO<sub>2</sub> methanation. *Catal. Today* **2021**, *362*, 35–46.

(75) Dong, J.; Wang, F.; Chen, G.; Wang, S.; Ji, C.; Gao, F. Fabrication of nickel oxide functionalized zeolite USY composite as a promising adsorbent for CO<sub>2</sub> capture. *Chin. J. Chem. Eng.* **2022**, *46*, 207–213.

(76) Subsadsana, M.; Sangdara, P.; Ruangviriyachai, C. Effect of bimetallic NiW modified crystalline ZSM-5 zeolite on catalytic conversion of crude palm oil and identification of biofuel products. *Asia-Pacific J. Chem. Eng.* **2017**, *12*, 147–158.

(77) Kadarwati, S.; Rahmawati, F.; Eka Rahayu, P.; Wahyuni, S.; Imam Supardi, K. Kinetics and mechanism of Ni/zeolite-catalyzed hydrocracking of palm oil into bio-fuel. *Indones. J. Chem.* **2013**, *13*, 77–85.

(78) Yaripour, F.; Mollavali, M.; Jam, S. M.; Atashi, H. Catalytic dehydration of methanol to dimethyl ether catalyzed by aluminum phosphate catalysts. *Energy Fuels* **2009**, *23*, 1896–1900.

(79) Ordonsky, V. V.; Sushkevich, V. L.; Schouten, J. C.; Van Der Schaaf, J.; Nijhuis, T. A. Glucose dehydration to 5-hydroxymethylfurfural over phosphate catalysts. *J. Catal.* **2013**, *300*, 37–46.

(80) Limlamthong, M.; Chitpong, N.; Jongsomjit, B. Influence of phosphoric acid modification on catalytic properties of Al<sub>2</sub>O<sub>3</sub> catalysts for dehydration of ethanol to diethyl ether. *Bull. Chem. React. Eng. Catal.* **2019**, *14*, 1–8.

(81) Rekoske, J. E.; Barteau, M. A. Kinetics and selectivity of 2-propanol conversion on oxidized anatase TiO<sub>2</sub>. *J. Catal.* **1997**, *165*, 57–72.

(82) Guo, W.; Kortenbach, T.; Qi, W.; Hensen, E.; Jan Heeres, H.; Yue, J. Selective tandem catalysis for the synthesis of 5-hydroxymethylfurfural from glucose over in-situ phosphated titania catalysts: insights into structure, bi-functionality and performance in flow microreactors. *Appl. Catal., B* **2022**, *301*, No. 120800.

## Recommended by ACS

### Efficient Catalytic Conversion of Glucose into Lactic Acid over Y-β and Yb-β Zeolites

Zheng Shen, Yalei Zhang, *et al.*

JULY 11, 2022  
ACS OMEGA

READ 

### Sulfonic Acid-Functionalized Brønsted Ionic Liquid-Catalyzed Isoprene Production via Prins Condensation between Methyl *Tert*-Butyl Ether and Formaldehyde in T...

Wenhao Xu, Siyu Yao, *et al.*

SEPTEMBER 22, 2022  
INDUSTRIAL & ENGINEERING CHEMISTRY RESEARCH

READ 

### Highly Dispersed and Stable Hydrotalcite-Derived NiCu/MgAlO Alloy Catalyst for Efficient Amination of Cyclohexanol to Cyclohexylamine in the Vapor Phase

Yanan Wei, He'an Luo, *et al.*

SEPTEMBER 27, 2022  
ACS SUSTAINABLE CHEMISTRY & ENGINEERING

READ 

### Process Optimization for Catalytic Oxidation of Dibenzothiophene over UiO-66-NH<sub>2</sub> by Using a Response Surface Methodology

Bijan Barghi, Allan Niidu, *et al.*

MAY 02, 2022  
ACS OMEGA

READ 

Get More Suggestions >